IOP Publishing Journal of Physics: Condensed Matter
J. Phys.: Condens. Matter **32** (2020) 234002 (15pp) https://doi.org/10.1088/1361-648X/ab74e4

The emergence of the local moment molecular spin transistor

Guanhua Hao[1], Ruihua Cheng[2] and P A Dowben[1]

[1] Department of Physics and Astronomy, University of Nebraska, Lincoln, NE, 68588-0299, United States of America
[2] Physics Department, Indiana University Purdue University, Indianapolis, 402 N Blackford Str. LD154, Indianapolis, IN 46202, United States of America

E-mail: rucheng@iupui.edu and pdowben1@unl.edu

Received 26 September 2019, revised 7 January 2020
Accepted for publication 11 February 2020
Published 12 March 2020

Abstract

Local moment molecular systems have now been used as the conduction channel in gated spintronics devices, and some of these three terminal devices might even be considered molecular spin transistors. In these systems, the gate voltage can be used to tune the molecular level alignment, while applied magnetic fields have an influence on the spin state, altering the magnetic properties, and providing insights to the magnetic anisotropy. More recently, the use of molecular spin crossover complexes, as the conduction channel, has led to devices that are both nonvolatile and have functionality at higher temperatures. Indeed, some devices have now been demonstrated to work at room temperature. Here, several molecular transistors, including those claiming to use single molecule magnets (SMM), are reviewed.

Keywords: molecular spintronics, spin transistors, molecular electronics, magneto-electric coupling

(Some figures may appear in colour only in the online journal)

1. Introduction

During the past few decades, 'molecular spintronics' has been actively pursued because of the possibility of making nanoscale devices that utilize the spin degree of freedom on the molecular scale [1–15]. This effort has been a combination of traditional molecular electronics with systems where the spin state matters, i.e. spintronics. Part of the motivation is the potential for addressing the complex grand challenge of manipulating magnetically ordered states by electrical means. The magnetic state may be switched through voltage control, potentially without large current densities or power consumption if the system is molecular, thus may lead to molecularly based nonvolatile device elements. This has considerable appeal. To date, most efforts at providing magnetic memory element solid-state devices have used magnetic spin valves or magnetic tunnel junction types of device structures. Many of the magnetic tunnel junction structures utilize inorganic dielectric thin films, combined with various magnetic layers, where large electrical current densities are required to reverse the direction of magnetization of one of the magnetic layers in the device structure [16–18]. This can be a big drawback.

Molecular systems have the possibility of providing a room temperature device on a length scale less than 10 nm while delivering low power nonvolatile local magneto-electric memory operations at peak (and only peak) current densities below 10^4 A cm^{-2}, i.e. reduced power consumption (potentially to be less than 3 aJ). The nonvolatility that is possible with these local moment or spin crossover molecular systems may require a structural change of some part of the molecular system or creation of suitable heteromolecular systems. This latter route seems promising as cooperative effects have now been observed [19]. The intermolecular cooperative effects, if dominant, suggest that room temperature nonvolatile molecular devices are likely to require write times that are longer than a nanosecond or, possibly, much longer. The molecular nature of such devices suggests that the devices themselves might be engineered to be flexible. Also of interest, but of

lesser practical value, are devices where conductance and spin state are manipulated by large magnetic fields.

To achieve the electric control of the magnetic properties on the molecular scale, especially for a single molecule (or just a few molecules) in a device structure, molecules with a large local magnetic moment have attracted considerable attention. A large variety of organometallic and metal organic molecules exist, with one or more transition metal or rare earth metal ions as inner magnetic core and organic ligands surrounding the core as the shell [20, 21], beginning with variants of $[Mn_{12}O_{12}(OAc)_{16}(H_2O)_4]$ [22–25]. The magnetic properties of these single molecule magnets (SMM) originate from the inner core, and often there exists a huge magnetic anisotropy within the molecule. The remanent magnetic moment, of the multiple metal atom core complexes, will depend on the alignment of the moments and the applied field. Single-ion single-molecule molecular magnets frequently retain the magnetic anisotropy of the multiple metal atom core complexes, and the dysprosium metallocene cation complex $[(Cp^{iPr5})Dy(Cp^{*})]^{+}(Cp^{iPr5}$, penta-iso-propylcyclopentadienyl; Cp^{*}, pentamethylcyclopentadienyl) exhibiting something akin to magnetic hysteresis up to 80 K [26].

As molecules, the single molecule molecular magnets (SMM) typically have a highest occupied molecular orbital (HOMO) to lowest unoccupied molecular orbital (LUMO) gap. Thus, condensed molecular systems have no free electron density, and there is no medium for exchange [27, 28], while intermolecular dipolar coupling is weak because of the separation between the metal cores. Not surprisingly, few are ferromagnetic or even antiferromagnetic as the condensed solid state films. There is no Stoner-like exchange [29], but rather these are local moment systems in the condensed phase and the exchange splitting, on the molecular scale, is going to be insensitive to temperature. This is distinct from the spin crossover complexes [30, 31], first noted as early as 1931 [32, 33], where the moment can vary from a low spin state, sometimes with zero net moment and thus exhibit diamagnetic behavior in the condensed solid state (as an ensemble of molecules) to a high spin state, thus showing moment paramagnetic behavior in the condensed solid state. In spite of the differences between the single molecule molecular magnets with multiple metal atoms, the single ion single molecule molecular magnets, and the spin crossover complexes in the high spin state, all are local moment molecular systems.

Chemical modification provides a desirable way to tailor the organic ligand, which makes selective bonding to a particular surface possible [34], thus optimizing the stability of the device and potentially can provide a specific bonding orientation. One can also change the magnetic core and so manipulate the magnetic properties of the molecule, without altering the structure significantly. Another way to switch the magnetization is through quantum tunneling. This phenomenon was observed in molecular crystals in 1996 [35, 36]. When an external magnetic field is applied along the easy axis of the molecular system, the degeneracy between m_s and $-m_s$ is lifted (with positive m_s being shifted up and negative shifted down), causing shifts in energy levels.

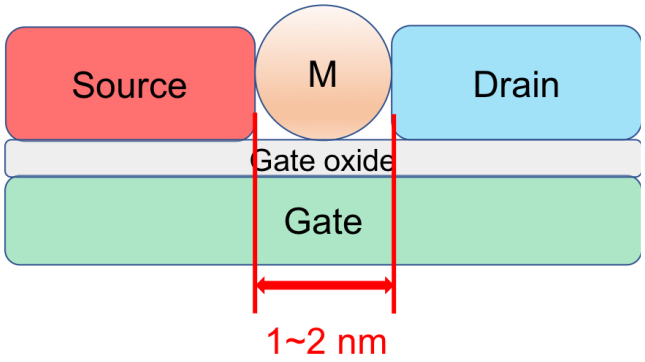

Figure 1. A schematic diagram of the single molecule transistor.

In spite of the many complications faced, there has been progress towards making a three-terminal molecular spintronic device and the molecular spin transistor has, in fact, now been realized. There has been much interest especially in molecular spin transistors where only a single molecule is addressed in the device. As reviewed here, these devices tend to show functionality only at very low temperatures, but more recently, molecular thin film devices have been shown to exhibit isothermal conductance switching even at room temperature.

2. Transport behavior of molecules in transistor geometry

The single molecule transistor represents a large variety of three-terminal devices where a single molecule is embedded into a gap between the source and drain electrodes (figure 1), and the gate adopted usually has the back-gated geometry, as reviewed elsewhere [27, 28]. Two types of the gate materials have been typically chosen: highly doped silicon substrates with SiO_2 grown on top or a native Al_2O_3 gate grown on top of aluminum. The choice of the gate material and thickness of the gate dielectric affects the break-down voltage of the gate oxide. The most challenging part is to fabricate nanogaps between the source and drain electrodes, with a separation width of only one molecule. One commonly-used approach for creating such a junction is electromigration where breaking of the conducting channel material is induced by large current [27, 28, 37–40], to form the gap between the nominal source and drain. After the gap is formed by electromigration, molecules are usually introduced into the junction via solution by drop-casting. In principle, such gaps can also be created as a break junction, where the conducting wire is broken by mechanical strain.

Once placed in the gap between source and drain of the transistor, SMMs are not just the semiconductor channel of the transistor, but a quantum dot with discrete energy levels. When a molecule comes in contact with the metal leads (the source and drain electrodes), the metal will screen or perturb the molecular orbitals [41, 42], causing a reduction of the HOMO and LUMO (lowest unoccupied molecular orbital) gap. This molecular orbital perturbation may be considered as molecule-lead (electrode) coupling, represented by Γ_s and Γ_d

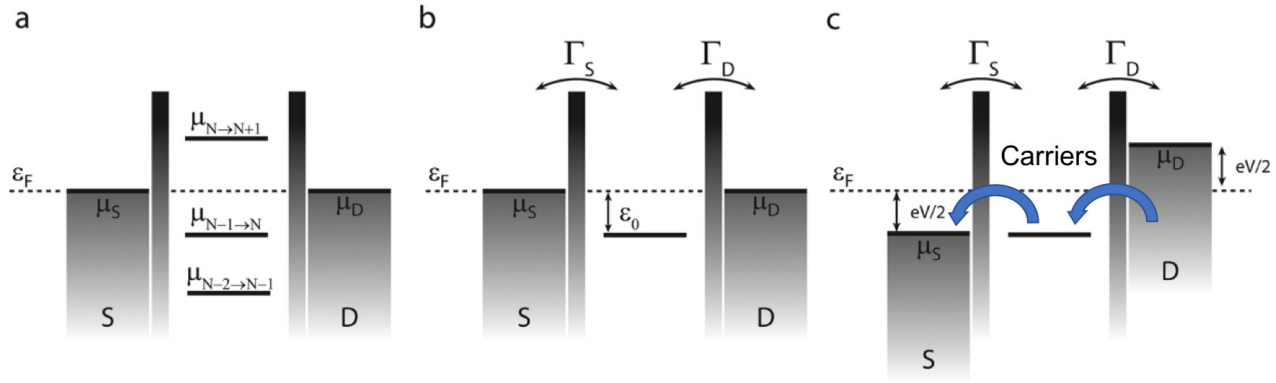

Figure 2. The chemical potential diagram of the molecular 'channel' respect to the leads without applying gate voltage (a) and (b) and under the influence of gate voltage V (c). Reproduced from [27] with permission of The Royal Society of Chemistry.

(here '*s*' stands for source and '*d*' stands for drain) in figure 2. These parameters affect tunneling rates and the overlap between the molecular wavefunction and the conduction electrons. The total coupling Γ, which is the sum of Γ_s and Γ_d, is an indicator of the broadening of the molecular levels due to the hybridization between the molecule and leads. As Γ gets bigger, the hybridization shifts both HOMO and LUMO closer to the Fermi Energy E_F, i.e. the HOMO–LUMO gap is reduced, as just noted, and the molecular levels broaden. Using electrochemical potential μ, molecular states can be considered in terms of μ(N), defined as the total energy difference between the N electron ground state and $N-1$ electron ground state (figure 2).

The tunneling transport in these molecular types of spintronic devices depends on the alignment between the chemical potentials of the molecule and leads (figure 2). In experiments, the transport properties are commonly characterized by measuring the change of current I or differential conductance dI/dV_{sd}, which could be obtained by taking numerical differentiation of the I–V plot, versus the source-drain bias V_{sd} under different gate voltages V_g at very low temperature (usually in mK range). The figures plotted from these measurements are often called stability diagrams.

Unsurprisingly, a lot of the molecular spin transistors exhibit very low currents due to the single molecule nature of the device and thus have limited total conductance. Transport in single molecular transistors occurs via electron tunneling from the source to the molecule which then tunnels out to the drain (co-tunneling). When the tunnel barrier resistance is much higher than the quantum of resistance ($h/e^2 = 25.8\,\mathrm{k\Omega}$), only one electron at a time can tunnel through the junction, and so places these devices in the framework of the single electron transistor [27]. While quantum conductance should go as $2e^2/h$, where the factor 2 comes from electron spin degeneracy, this latter spin degeneracy is lifted when the molecule has a large magnetic moment.

When the reduction of the HOMO–LUMO gap is still small, i.e. in case of the weak coupling between the local moment molecule and the electrodes, performing such experiments will show some interesting features: at low gate voltage V_g, there exist several regions of source-drain voltage, V_{sd}, and V_g where there is no current (zero conductance) and this is referred to as Coulomb blockade. Coulomb blockade shows up as diamond shaped bounded regions (named Coulomb diamonds) on differential current plots as a function of gate voltage V_g and source-drain voltage, V_{sd} (figure 3). Within each Coulomb diamond, the charge of the molecule is fixed to an integer number, and adjacent diamonds differ by only one charge (electron or hole).

Bright areas in the current plots (figure 3(b)) denote single electron tunneling (SET) region, where the transistor is in its 'ON' state. The points connecting adjacent Coulomb diamonds are degeneracy points, which means at specific choices of V_{sd} and V_g, the energy between two charge states of the molecule, are the same. The gate voltage serves as a means to shift and 'tune' the molecule chemical potential. When $V_{sd} = 0$, μ_s is aligned with μ_d. If the molecular level is shifted at the same chemical potential level as the leads (which is at the degeneracy point), electrons can tunnel through the molecule, resulting in a non-zero conductance signal, SET could occur. When applying a non-zero voltage V_{sd}, between the source and drain leads, the potential will shift the source chemical potential μ_s up by $\frac{1}{2}e\,|V_{sd}|$, combined with pulling the drain μ_d down by the same value, resulting in a bias window with a width of $e|V_{sd}|$ (figure 2(c)). When the molecular level is correctly tuned within this bias window region, single electron transport will occur.

The current, when plotted as differential conductance inside the SET region, the parallel lines to the diamond edges (which could be seen in figure 3(c)) are related to the contribution of the conductance due to excited states [27]. These excitations can have an origin related to charge, phonons (vibrational), and a variety of other optical excitations.

2.1. Mn_{12} family of local moment complexes

Among the most studied SMM is the 'Mn_{12}' large spin moment class of molecules, discovered by Lis in 1980 [22], which contain a core of 12 Mn atoms surrounded by acetate ligands. [$Mn_{12}O_{12}(O_2C\text{-}R\text{-}SAc)_{16}(H_2O)_4$], or '$Mn_{12}$ acetate' has, in fact, been used to make single molecule transistors. Absent ligand contributions, the molecule has a total spin S = 10, with an Ising type anisotropy barrier of around 6 meV [25, 43]. Heersche *et al* [44] investigated the transport properties of two Mn_{12} derivatives ($Mn_{12}O_{12}(O_2C\text{-}R\text{-}SAc)_{16}(H_2O)_4$] where $R = C_6H_4$, $C_{15}H_{30}$), at a temperature of

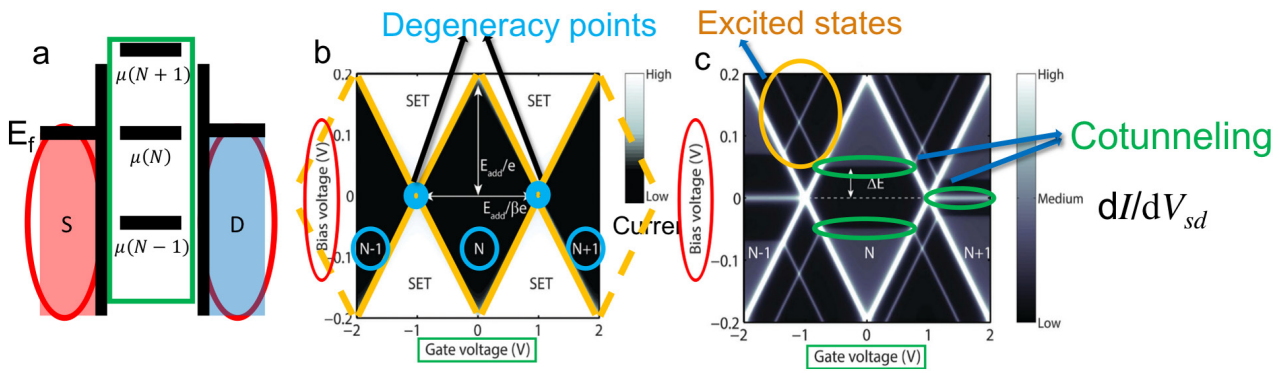

Figure 3. Schematic diagram of the current and differential conductance response for a single electron molecular transistor. (a) Chemical potential diagram of the molecule island. (b) Current map versus bias voltage and gate voltage. (c) Differential conductance plotted versus bias voltage and gate voltage. Image (b) and (c) are reproduced from [27] with permission of The Royal Society of Chemistry.

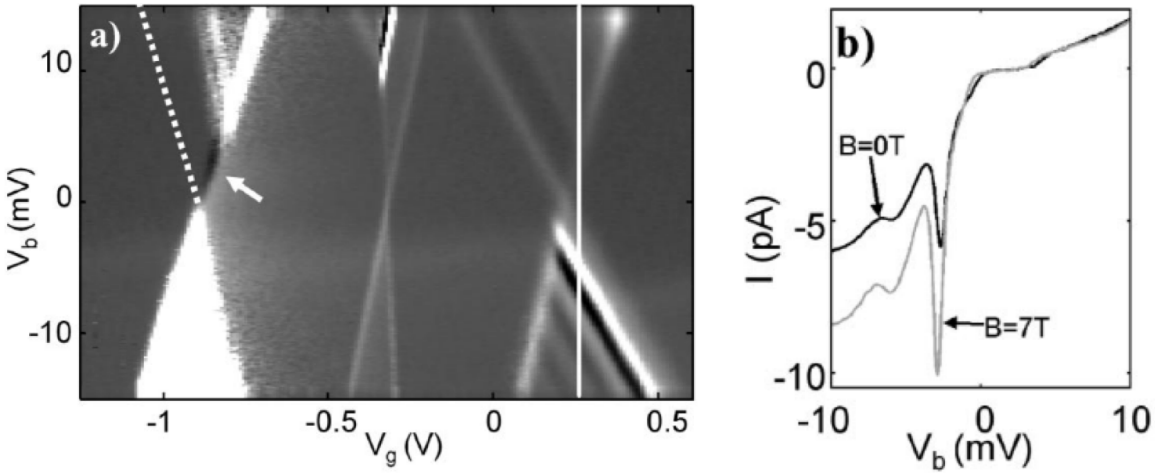

Figure 4. (a) Differential conductance stability diagram in gray scale of the Mn_{12} derivative ($Mn_{12}O_{12}(O_2C\text{-}R\text{-}SAc)_{16}(H_2O)_4$], taken at a temperature of 3 K. (b) The current versus voltage (*I*–*V*) curve, at the gate voltage indicated by white line at the left in panel (a). Reprinted figure with permission from [44]. Copyright (2006) by the American Physical Society.

3 K, in 2006. In their device, they used thiol groups as the outer ligand to ensure a strong affinity to the gold surface so that the molecule is robustly tethered to the Au electrodes, while still weakly perturbed by the metallic contacts. Some interesting features appear in the differential conductance plots including regions with complete current suppression and negative differential conductance, as seen in figure 4. At the degeneracy point, indicated on the left side of figure 4(a), the current is fully suppressed at some positive source-drain bias voltages (above the dashed line in figure 4(a)) and restored at an excitation which appears 5 meV higher. Two excitations at 2 meV (positive differential conductance) and 3 meV (negative differential conductance) are evident in the right side of figure 4(a). The current (*I*) versus source-drain bias plot shows this negative differential conductance feature as well (figure 4(b)). Conventional Coulomb blockade theory is an inadequate explanation [44], and this may be related to the charge induced distortion of the local spin state. In the context of their model, Heersche *et al* [44] suggested that upon adding or subtracting one electron, the spin selection rule $|\Delta S|, |\Delta S_z| = 1/2$ should apply for each energy allowed sequence. The subsequent sequential tunneling may result in the accumulation of a certain excited state while the relaxation of the moment could only occur by quantum tunneling of the magnetization, which is slow. Transport is thus hindered, and negative differential conductance and complete current suppression may occur [44]. Heersche *et al* [44] also observed enhancement of the current when an external magnetic field is applied to the device, but no specific conclusion was drawn.

Later, Jo *et al* [45] performed single molecule transistor measurements on $Mn_{12}Ac$ and $Mn_{12}Cl$ derivatives (Mn_{12} derivatives ($Mn_{12}O_{12}(O_2CCH_3)_{16}(H_2O)_4$, i.e. 'MnAc' and $Mn_{12}O_{12}(O_2CCHCl_2)_{16}(H_2O)_4$, i.e. 'MnCl'), mainly focusing on the magnetic field dependence at temperature less than 300 mK. For the transistor, based on $Mn_{12}Ac$ (figures 5(a) and (b)), two excitations were observed at zero magnetic field B (yellow and green arrows). Upon applying a magnetic field of 8 T, neither of the peaks (indicated by the yellow and green arrows in figures 5(a) and (b)) have split (into the expected two peaks), meaning no simple Zeeman splitting occurs with this 'MnAc' derivative [45], although the shift of one feature (indicated by the yellow arrow, figure 5(b)) to higher energy is indicative of a Zeeman like effect. For $Mn_{12}Cl$ transistor (figures 5(c) and (d)), Zeeman splitting is much more evident

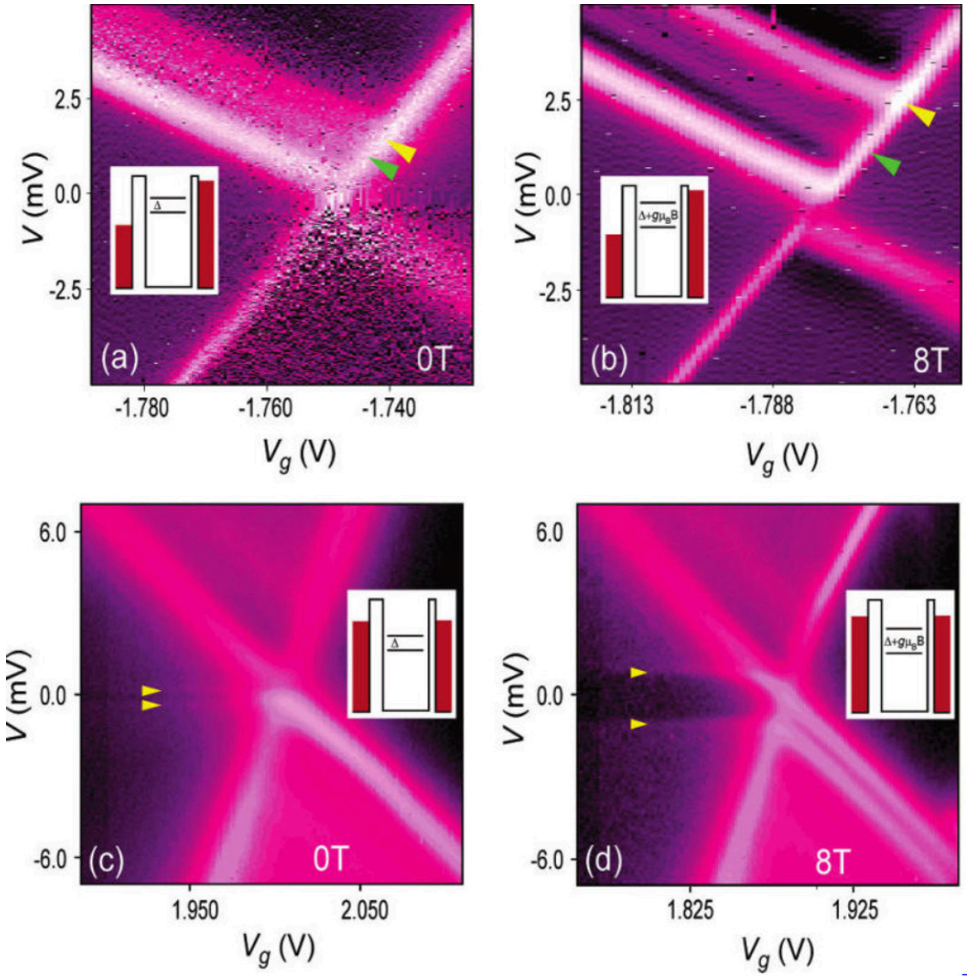

Figure 5. (a) and (b) The differential conductance stability plots for a '$Mn_{12}Ac$' local moment molecular transistor, taken at $B = 0$ T and $B = 8$ T. (c) and (d) The differential conductance stability plots for $Mn_{12}Cl$ local moment molecular transistor. The data was taken a temperature in the region <300 mK. Arrows indicating excited states. Reprinted with permission from [45]. Copyright (2006) American Chemical Society.

in the changes that occur in Coulomb blockade region of the differential conductance plot from figures 5(c)–(d) (as indicated by the changing positions of the states indicated by the yellow arrows) [45].

The presence of splitting in the conductance plots, at zero applied magnetic field, is certainly possible and is observed in the local moment of $Mn_{12}O_{12}(O_2CCH_3)_{16}(H_2O)_4$, i.e. 'MnAc' system, as seen in figure 6(a) [45]. A magnetic anisotropy barrier, figure 6(b) [45], is challenged in the presence of an applied magnetic field as the splitting, in the conductance plots, decreases with increasing applied field. The steps in the plot of differential conductance, in figure 6(a) may be related to different available spin states, and the behavior overall is indicative of a magnetic anisotropy as discussed next.

3. The influence of magnetic anisotropy

Molecular spin transistors using SMM has been studied in a large variety of molecules [27, 28, 38, 39] and device characteristics can be affected by more than just the spin and charge state. The magnetic property of a single molecule magnet might be roughly described as the following Hamiltonian (omitting thermal effects and higher order terms for simplicity) [20, 27, 28]:

$$H = DS_z^2 + E\left(S_x^2 - S_y^2\right) + g\mu_B\mu_0 \boldsymbol{S}\cdot\boldsymbol{H}. \quad (1)$$

Here S_x, S_y and S_z are spin operators in the three orthogonal directions, D is the axial magnetic anisotropy while E is the transverse magnetic anisotropy. Usually $|D| \gg |E|$, which results in a large magnetic anisotropy in z direction (easy axis along S_z direction). The magnetic anisotropy means that SMM, with the ground state of spin S, can be divided into $(2S + 1)$ discrete energy values for different m_s (from $-S$ to S) along z direction. The sign of the first term D is negative, so the potential energy of the ground state forms a double well potential, so that states between m_s and $-m_s$ are separated by an anisotropy barrier. The last term in Hamiltonian is associated with the Zeeman energy that occurs when an external magnetic field is applied to the system.

Due to the presence of the anisotropy barrier, in order to make a transition from m_s to $-m_s$, i.e. to reverse the magnetization direction of the molecular local moment, one has to overcome the potential barrier with height $\left|DS_z^2\right|$, this could be done by the thermal activation or application of a sufficiently

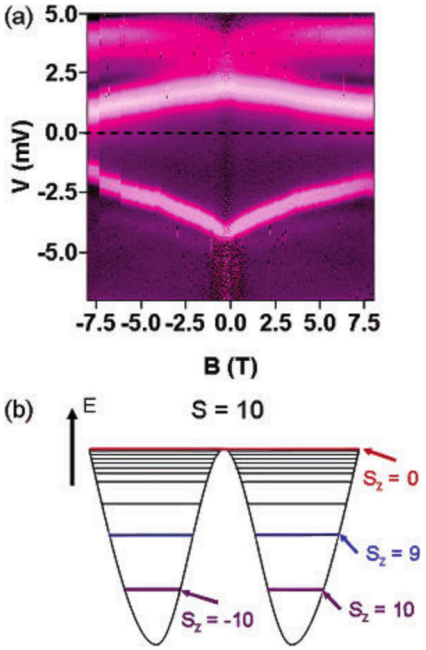

Figure 6. (a) The nonlinear evolution of the zero field split peaks (indicative of a large local moment magnetic system) as B sweeping for the molecular transistor based on the Mn_{12} derivatives $(Mn_{12}O_{12}(O_2CCH_3)_{16}(H_2O)_4$, $Mn_{12}Ac$, taken at in the temperature region <300 mK, and (b) energy diagram of $S = 10$ state in Mn_{12} molecule. Reprinted with permission from [45]. Copyright (2006) American Chemical Society.

large magnetic field [45]. The relaxation time will increase in an exponential fashion as temperature goes down. For the $Mn_{12}O_{12}(O_2C\text{-}R)_{16}(H_2O)_4$ class of Mn_{12} molecules, the local magnetization state is extremely long lived at temperatures in the region of 2 K [21].

3.1. The Fe_4 molecular complexes

Three terminal local moment molecular spin devices, with a Fe_4 metal core, have also been investigated (by Zyazin *et al* [46] and Burzuri *et al* [47]), much in the same was at the Mn_{12} molecular complexes just discussed. Three derivatives of the Fe_4 metal core molecule $[Fe_4L_2(dpm)_6]$ (Hdpm = 2,2,6,6-tetramethyl-heptan-3,5-dione) were studied with the ligand moieties $H_3L = R\text{-}C(CH_2OH)_5$ with R = phenyl (i.e. 'Fe_4Ph') and R = 9-(acetylsulfanyl)nonyl (i.e. 'Fe_4C_9SAc') [46], as well as $[Fe_4L_2(dpm)_6] \cdot Et_2O$ (H_3L = 2-hydroxymethyl-2-phenylpropane-1,3-diol) [47]. These complexes contains four Fe^{3+} ions, with one Fe^{3+} antiferromagnetically coupled to the other three and together the metal core is encapsulated in a hydrophobic shell made by ligands resulting in the total spin $S = 5$, as indicated in figure 7, and magnetic anisotropy barrier of 16 K (roughly 1.3 to 1.4 meV) [46].

With a single Fe_4Ph or Fe_4C_9SAc complex, embedded between source and drain, in a gated three terminal device (like figure 1), interesting transport properties were observed at 1.6 K [46]. Although the yield of successful devices was low [46, 47], the signature of Coulomb blockade was observed [46, 47], but so was the observed inelastic cotunneling, with the data for the single Fe_4Ph derivative shown in figure 8(a). The regions of SET are also indicated.

The applied magnetic field dependence, shown in figures 8(b) and (c) for the single Fe_4Ph derivative, was related to the zero-field splitting of adjacent charge states (figure 7). Within each Coulomb blockade area, the charge of the molecule was fixed, thus the magnetic anisotropy is fixed in the left and right region respectively of the differential conductance plot. The excitation energy of the left charge states is close to the zero-field splitting of the bulk crystal, assumed to be the neutral state with $|D|$ (of equation (1)) around 0.06 meV. Under the influence of an increasing applied magnetic field B, the increase of the excitation energy is linear (figures 8(b) and (d)), indicating a small angle between B and S [46]. Since a substantial angle will increase the transverse anisotropy component and can lead to a nonlinear behavior, which was observed for the Fe_4C_9SAc complex [46] and the Fe_4 complex $[Fe_4L_2(dpm)_6] \cdot Et_2O$ (H_3L = 2-hydroxymethyl-2-phenylpropane-1,3-diol) [47]. The gate voltage will change the charge state of the molecule, changing its magnetic properties. Upon adding one electron into the molecule, the magnetic field dependence of the $N + 1$ charge state (figures 8(c) and (e)) suggests a $|D|$ around 0.09 meV.

As indicated above, the evolution of the excitation energy, under applied magnetic field B, is related to the angle between **B** and **S**. Burzurí *et al* [47] performed angular dependent magnetic field studies on the similar Fe_4 complex ($[Fe_4L_2(dpm)_6] \cdot Et_2O$, where again Hdpm = 2,2,6,6-tetramethyl-heptan-3,5-dione and H_3L = 2-hydroxymethyl-2-phenylpropane-1,3-diol) spin transistors [47]. The changes in the energy levels, as a function of applied magnetic field, are clearly nonlinear in a zero bias Coulomb feature, in the differential conductance plots. The simulations (figure 9(b)) suggest that the changes, with magnetic field, become more nonlinear as the angle between **B** and **S** increases, consistent with experiment (figure 9(c)). The zero bias Coulomb feature, in the differential conductance plots, does show a deviation as the direction of the applied B field, relative to the device, is rotated by 90 degrees, providing more direct proof of the magnetic anisotropy [47]. Kondo correlations were also observed [46, 47], and we discuss Kondo effects next.

4. Kondo effects in nominally single molecule transistor

Higher order tunneling processes will show up when the coupling, i.e. interaction, between the molecule and the electrodes is enhanced [28, 46–49]. In 2002, two papers [48, 49], published together in Nature, highlighted Kondo effects in molecular spin transistors. Park *et al* [48] made transistors with two similar Co based molecular complexes (Co bonded to two polypryridyl ligands, with thiol end groups, i.e. $Co(tpy\text{–}(CH_2)_5\text{–}SH)_2$ and $Co(tpy\text{–}SH)_2$). One of the goals of this work was to change metal-organic complex coupling to the metal electrodes [48]. This change in the interaction of the $Co(tpy)_2$ molecular complex with the electrode, was affected by

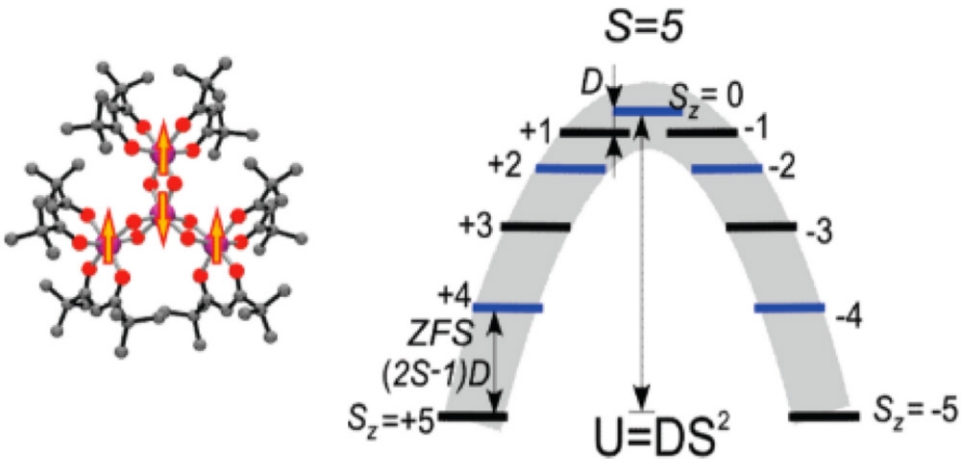

Figure 7. The generalized $[Fe_4L_2(dpm)_6]$ molecule on the left and the spin state anisotropy diagram on the right, for such molecular systems with an Fe_4 core, where the zero-field splitting, is denoted by ZFS. Reprinted with permission from [46]. Copyright (2010) American Chemical Society.

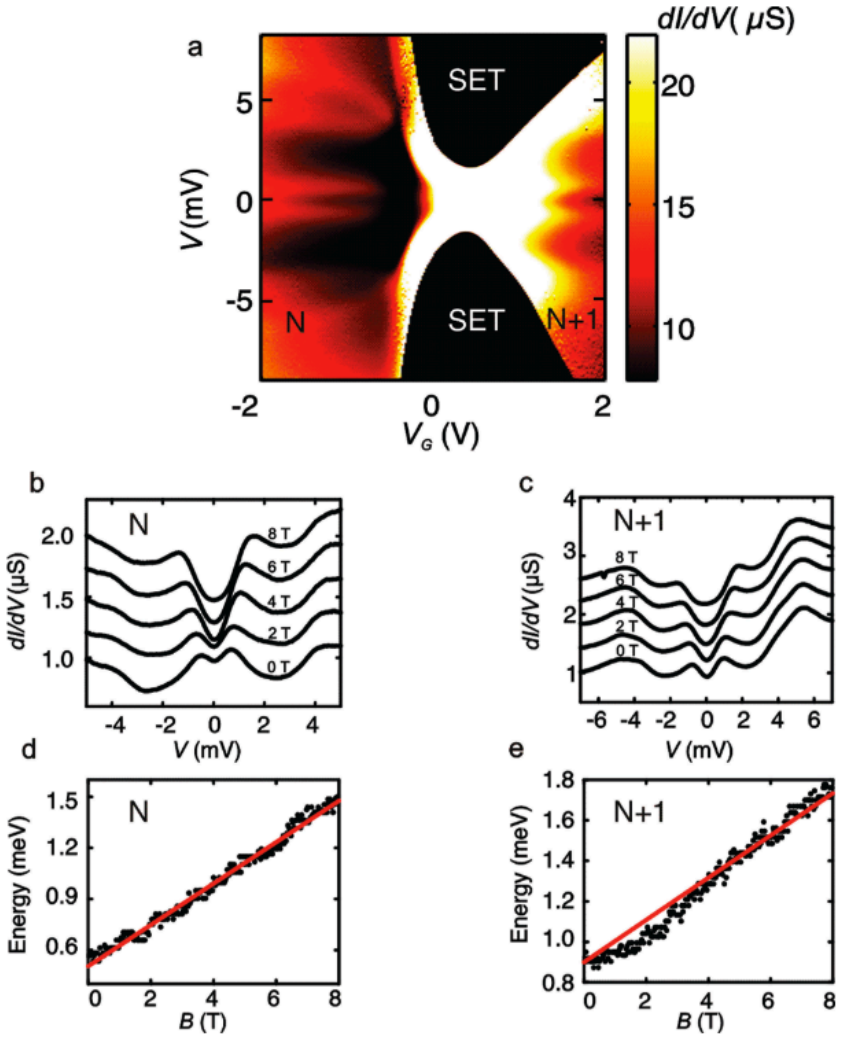

Figure 8. Differential conductance plots for the $[Fe_4L_2(dpm)_6]$, i.e. an Fe_4 complex, molecular spin transistor and B field dependency study, taken at 1.6 K. SET in (a) denoted the region of SET. Reprinted with permission from [46]. Copyright (2010) American Chemical Society.

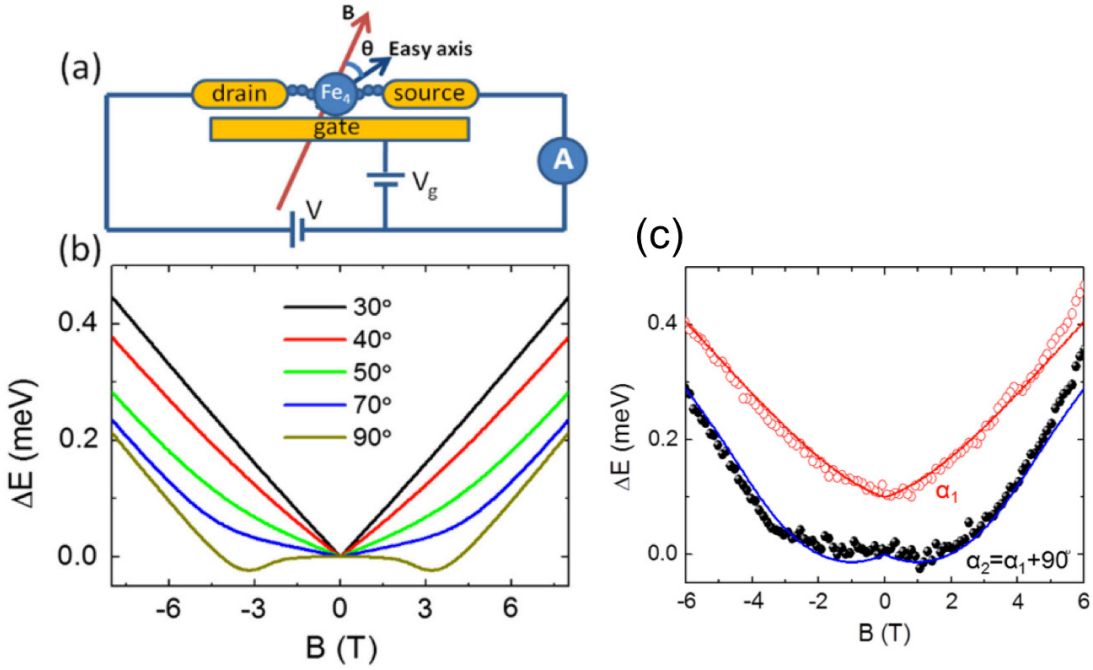

Figure 9. (a) The schematic of the molecular spin transistor, with the possible variation between the easy axis and applied magnetic field indicated, based on the Fe_4 complex (complex $([Fe_4L_2(dpm)_6] \cdot Et_2O)$, where H_3L = 2-hydroxymethyl-2-phenylpropane-1,3-diol)). (b) The model of the shift in energy level, with applied magnetic field for various angles (only considering the DS_z^2 and Zeeman term). (c) The experimental results of a zero bias Coulomb feature in the differential conductance plots, as a function of applied magnetic field **B** at two different angles, taken at 1.9 K. Reprinted figure with permission from [47]. Copyright (2012) by the American Physical Society.

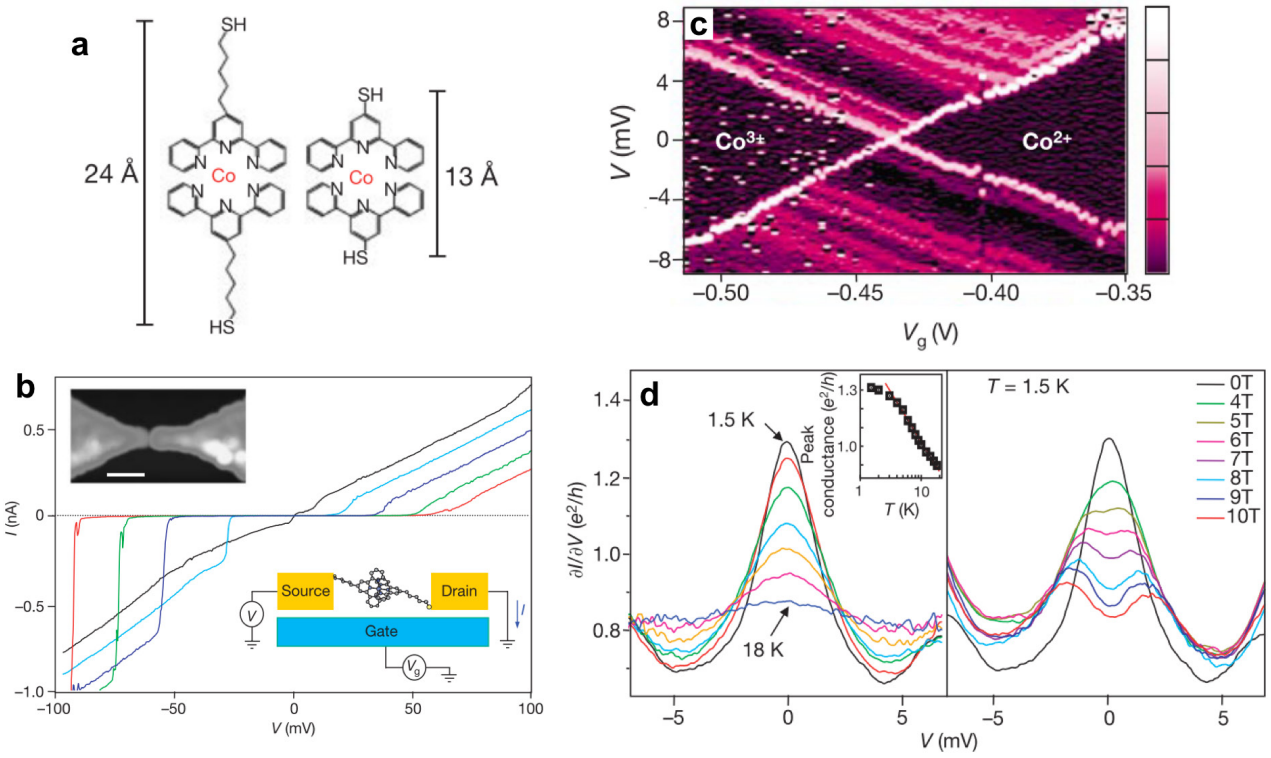

Figure 10. (a) The long and short Co complex molecules $Co(tpy–(CH_2)_5–SH)_2$ and $Co(tpy\text{-}SH)_2$. (b) Device schematics and *I–V* curve showing the $Co(tpy–(CH_2)_5–SH)_2$ transistor conductance can be turned on and off. (c) The differential conductance diagram for $Co(tpy–(CH_2)_5–SH)_2$, with the long chain alkane thiol, as a function of source drain voltage (vertical) and gate voltage (horizontal). (d) The temperature evolution of the zero bias Kondo peak, on the left and the magnetic field dependence on the right, for $Co(tpy–SH)_2$. Reprinted by permission from Springer Nature Customer Service Centre GmbH: Nature, Electronics and the single atom, [48]. Copyright © 2002, Springer Nature.

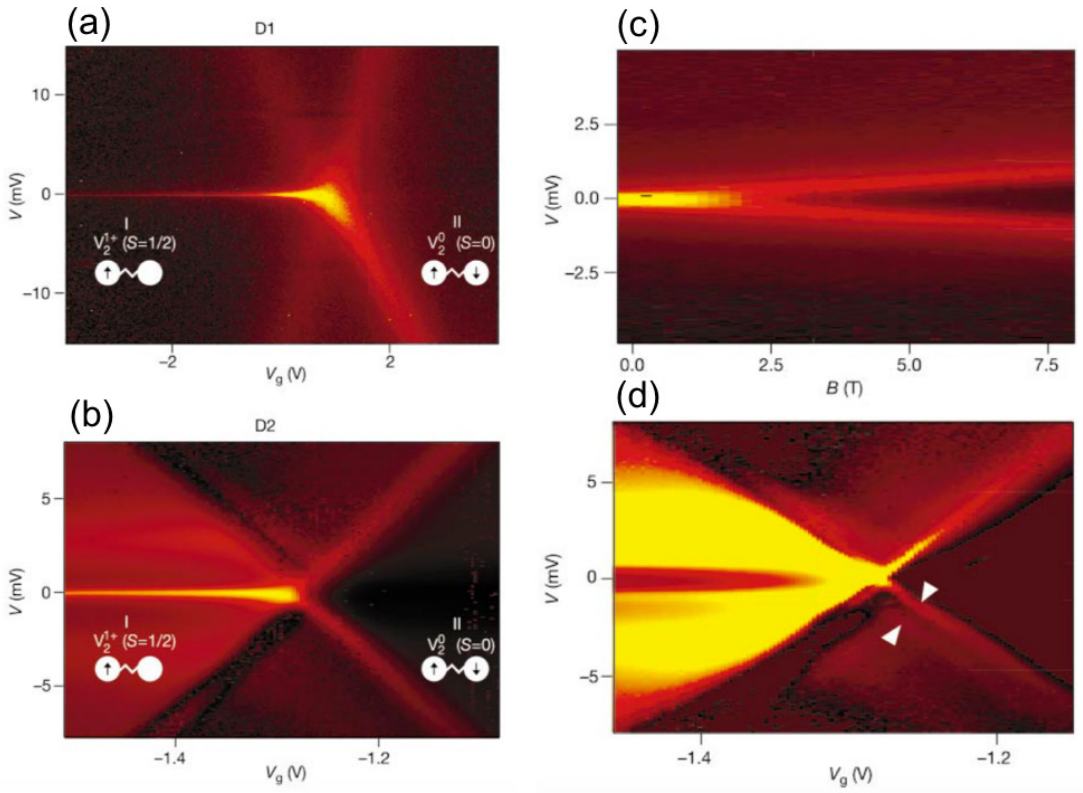

Figure 11. (a) and (b) The differential conductance plots, for the V_2 molecule (N, N′, N″-trimethyl-1,4,7-triazacyclonane)$_2$-V_2(CN)$_4$(μ-C_4N_4)), showing Kondo resonance in two individual devices (a) and (b). The inserted diagrams indicate the charge and spin state. (c) The Zeeman splitting under B field of the Kondo resonance peak and the differential conductance plot versus gate and source drain voltage, taken at an applied magnetic field of 8 T. The data were acquired at 300 mK. Reprinted by permission from Springer Nature Customer Service Centre GmbH: Nature, Electronics and the single atom, [49]. Copyright © 2002, Springer Nature.

changing the length of the alkane thiol groups (−$(CH_2)_5$–SH versus −SH) in ligands, as indicated in figure 10(a) [48]. With the long alkane thiol moiety (−$(CH_2)_5$–SH), the Co(tpy)$_2$ molecular complex retained the behavior typical of a single electron transistor (figure 10(c)), yet with a voltage control of the charge and spin state.

With the shorter alkane thiol moiety (−SH), the coupling of the Co(tpy)$_2$ molecular complex was enhanced and a zero-bias conductance Kondo resonance was observed (figure 10(d)) [48], as was observed for [Fe_4L_2(dpm)$_6$] complexes discussed above [46, 47]. Moreover, the Kondo resonance peak, for Co(tpy-SH)$_2$, splits under an applied magnetic field with spacing $2g\mu_B H$, as seen in figure 10(d), [48]. The Kondo temperature was estimated to be around 10–25 K.

Liang *et al* [49] investigated a single electron transistor fabricated with a divanadium (V_2) complex N, N′, N″-trimethyl-1,4,7-triazacyclonane)$_2$-V_2(CN)$_4$(μ-C_4N_4), in a device much like that illustrated in figure 1. The coupling is strong enough to observe a Kondo resonance within the left Coulomb diamond of the differential conductance plot (figures 11(a) and (b)). Under the application of a magnetic field, the Kondo resonance undergoes Zeeman splitting, indicating a lifting of the spin 1/2 degeneracy at negative gate bias (figures 11(c) and (d)). Upon adding one electron into the molecule, through an applied voltage, the spin degeneracy is lost and the Kondo resonance disappears [49]. The Kondo effect, for N, N′, N″-trimethyl-1,4,7-triazacyclonane)$_2$-V_2(CN)$_4$(μ-C_4N_4), was retained up to 30 K.

Meded *et al* [50] studied the electric control of an Fe(II) spin crossover complex $[Fe^{II}(bpp)_2]^{2+}$ (bpp = 2, 6-bis(pyrazol-1-yl)pyradine) in three-terminal geometry. Their DFT calculation showed that when the molecule charge falls to $q = +2$, the low spin state (LS) is more stable; for the charge neutral $q = 0$, the high spin state (HS) becomes the ground state. Thus adding two electrons will trigger a transition from the LS state to the HS state, and the addition of electrons could be achieved by the gate voltage. Experimental results showed that upon adding electrons, the zero bias differential conductance changed, indicating a spin state transition (figure 12). As temperature goes up, the variation of the conductance is reduced but as seen in figure 12(b), Kondo effects are evident [50]. The Kondo model fits, to the zero bias differential conductance data, suggest a Kondo temperature of 56 K for this $[Fe^{II}(bpp)_2]^{2+}$ (bpp = 2, 6-bis(pyrazol-1-yl)pyradine) device [50].

5. Probing the nuclear spin

The single molecule magnet $TbPc_2$, where a single Tb^{3+} ion is sandwiched by two organic phthalocyanine (Pc) ligands, has also attracted attention [51–55]. Part of the appeals is that this metal-phthalocyanine molecule has a magnetic ground

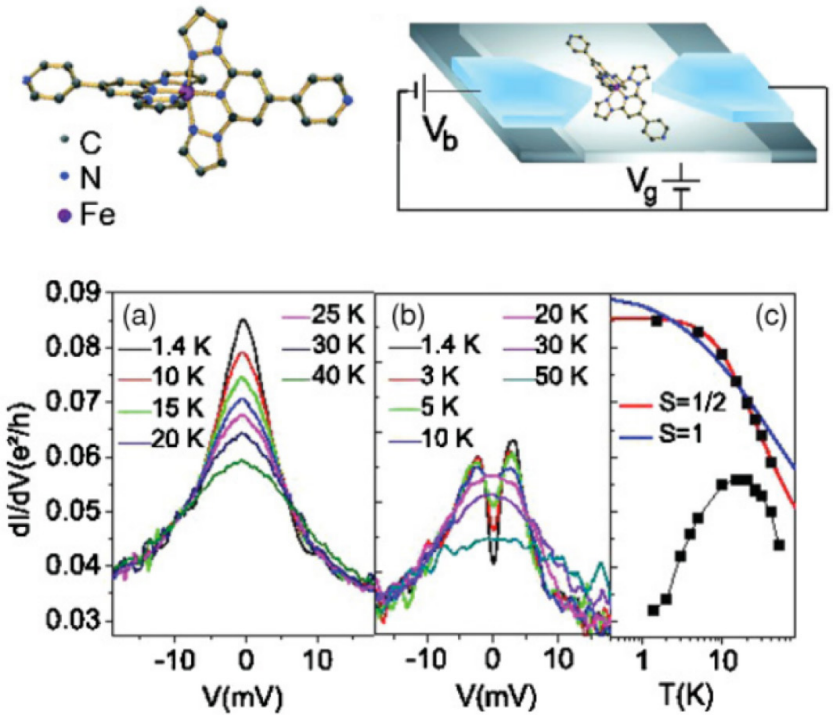

Figure 12. Top: the spin crossover complex molecule and device geometry for the single $[FeII(bpp)_2]^{2+}$ molecular spin crossover channel transistor. (a) and (b) Temperature dependence of differential conductance versus bias voltage, near zero bias, showing the temperature dependence of the Kondo peak. (a) Data taken for a gate voltage of 2.2 V, while (b) is taken for a gate voltage 3.2 V. (c) Temperature dependence of the zero-bias conductance in (a) and (b). Reprinted figure with permission from [50]. Copyright (2011) by the American Physical Society.

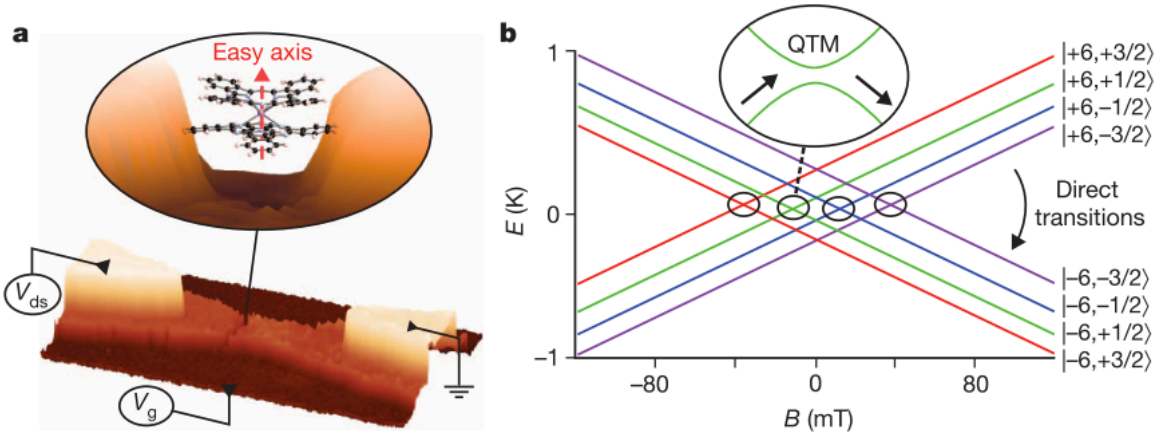

Figure 13. (a) The $TbPc_2$ molecular spin transistor and (b) the energy diagram of spin reversal processes. In (b), two different mechanisms (quantum tunneling and direct reversal) are indicated. Reprinted by permission from Springer Nature Customer Service Centre GmbH: Nature, Electronics and the single atom, [51]. Copyright © 2012, Springer Nature.

state of J = 6 with very strong uniaxial magnetic anisotropy, along the normal to the phthalocyanine plane (as indicated in figure 12(a)), due to the strong spin-orbit coupling of the complex. When connected to an electric bias, current flows more favorably through the π conjugated Pc ligands [51]. Because of the huge energy gap from the $J_z = \pm 6$ ground state to the first excited state (corresponding to a few hundred Kelvin), the molecule will stay in a stable ground state when experiments are performed at lower temperatures (<5 K) and small magnetic fields (<10 T). Due to the hyperfine coupling between the nuclear spin $I = 3/2$ and Tb^{3+} local moment, due to unpaired electron spins, the ground state $J_z = +6$ of this molecule will split into four hyperfine states with $|J_z, I_z> = |+6, +3/2>$, $|+6, +1/2>$, $|+6, -1/2>$, and $|+6, -3/2>$, and similarly for $J_z = -6$, as indicated in figure 12(b). At small applied magnetic fields, a transition could occur, for example between $|+6, +1/2>$ and $|-6, +1/2>$ via quantum tunneling, at the avoided energy level crossings, while at higher magnetic fields, direct relaxation is possible, leading to the reversal of J (figure 13(b)) [51].

Vincent *et al* [39] explored $TbPc_2$ in a three-terminal molecular transistor and achieved the probing of the nuclear spin via electrical means and a direct proof of quantum tunneling of magnetization (QTM). Sweeping the magnetic

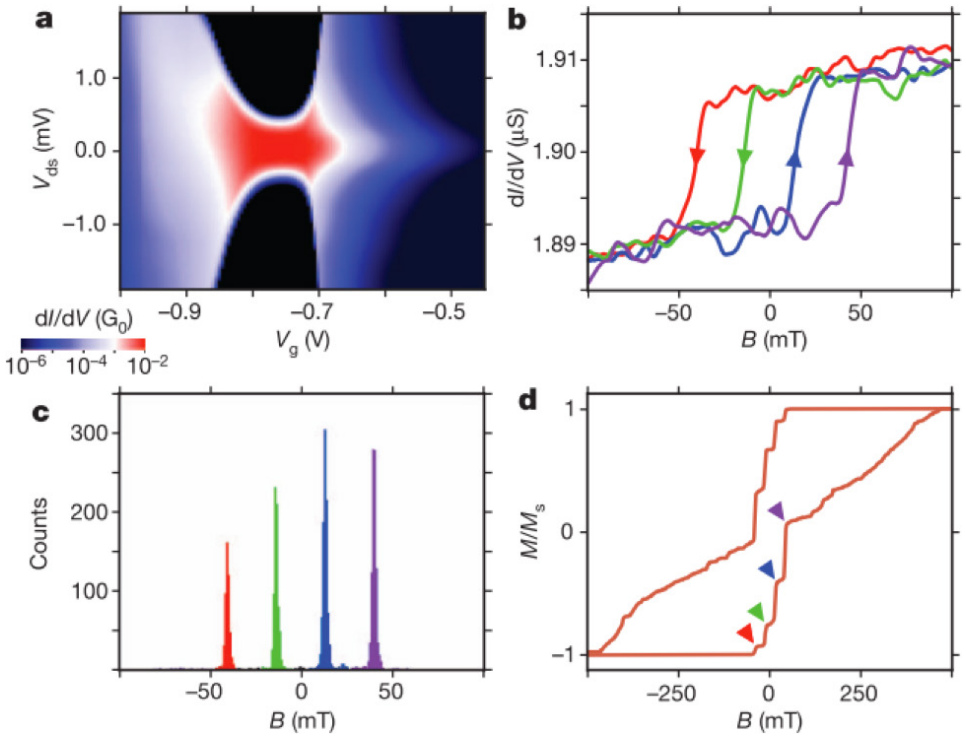

Figure 14. The conductance characteristics of $TbPc_2$ transistor at temperatures less than 5 K. (a) The differential conductance plot versus gate and source-drain voltage while (b) is the applied magnetic field B dependence for a gate voltage of $V_g = -0.9$ V and source drain voltage of $V_{sd} = 0$ V, where the arrows indicate the direction of magnetic field sweep. The abrupt jumps were associated with QTM. (c) Statistical results from 11 000 trials sweeping the magnetic field, showing the robustly discrete QTM. (d) Hysteresis generated by integration of 1000 trials, with the arrows indicating the four discrete magnetic fields associated with QTM events (−40 mT (red), −14 mT (green), 14 mT (blue) and 40 mT (purple)). Reprinted by permission from Springer Nature Customer Service Centre GmbH: Nature, Electronics and the single atom, [51]. Copyright © 2012, Springer Nature.

field near the degeneracy point, abrupt jumps of differential conductance, *dI*/*dV*, were observed at four discrete values of magnetic field B (figure 14(b)), associated with the reversal of Tb^{3+} magnetic moments, resulting from QTM [52]. Statistical studies verified the precision of these applied magnetic field measurements (figure 14(c)). Later, Thiele *et al* utilized this read-out mechanism and achieved some control of the hyperfine interactions using an electric field pulse [52]. Other differential conductance change experiments for $TbPc_2$ [53], provided evidence of the direct reversal of magnetization, at higher magnetic fields, rather than quantum tunneling as well as evidence for electron phonon coupling.

We suggest that equivalent complex, with praeseodynium instead of terbium, might be interesting for comparison, as ferromagnetism in Pr arises from the nuclear moment, through the hyperfine interaction, at extremely low temperatures.

6. Molecular spin transistor using spin crossover molecular thin films

The molecular transistors, discussed so far, have not been accompanied by any evidence of nonvolatile switching at room temperature: the device measurement were carried out at temperatures below 30 K. To obtain functional molecular spintronic devices, which are operational at temperatures closer to room temperature, molecular systems exhibiting a robust spin transition have begun to attract increasing attention [1–15]. The spin crossover phenomenon, representing transitions between two distinguishable spin states, occurs in a large variety of 3*d* transition metal molecular compounds [30, 31]. The two electronically distinct spin states, usually called low spin state (LS) and high spin state (HS), can be reversibly switched. Various external stimuli can trigger this spin transition, such as temperature, pressure, light, but above all electric field [7, 8, 15, 39, 43, 44]. From a practical point of view, if spin crossover molecules are expected to be used for solid state devices, there must be a way to 'easily' sense the change of the spin state so that the state could be 'read', and among the most desirable read mechanisms would be a conductance change, as seen in the experiments discussed above. The spin transition is seen to be accompanied by a conductance change [4, 5, 7, 8, 12–15, 56, 57], as reviewed by Lefter *et al* [15]. Furthermore, isothermal changes in the electronic structure and spin state have now been achieved for the Fe (II) spin crossover complex $[Fe\{H_2B(pz)_2\}_2(bipy)]$ [5, 9], $[Fe(trz)_3](BF_4)_2$ (trz = triazole)] [14], $[Fe(phen)_2(NCS)_2]$ [7] and $\{Rb_{0.8}Mn[Fe(CN)_6]_{0.93} \cdot 1.62H_2O\}$ [12] at or near room temperature. More recently, magnetoelectric effects have been observed for $NiCl_2$–$4SC(NH_2)_2$ [58], $CuCl_2{\cdot}2[(CH_3)_2SO]$ [59] and $[Mn^{3+}(pyrol)_3(tren)]$ [60], which certainly has device implications [61], if this can be demonstrated reliably at room temperature.

Zhang *et al* [62] showed that for spin crossover molecular films of $[Fe(H_2B(pz)_2)_2bipy]$, where

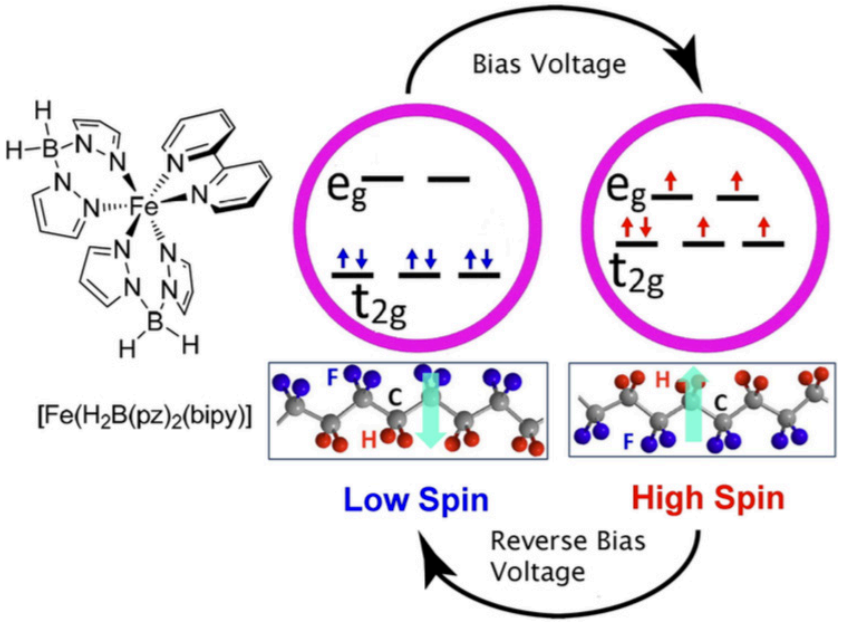

Figure 15. Schematics of voltage control of spin state switching by ferroelectric substrate polarization change. Reprinted from [56], with the permission of AIP Publishing.

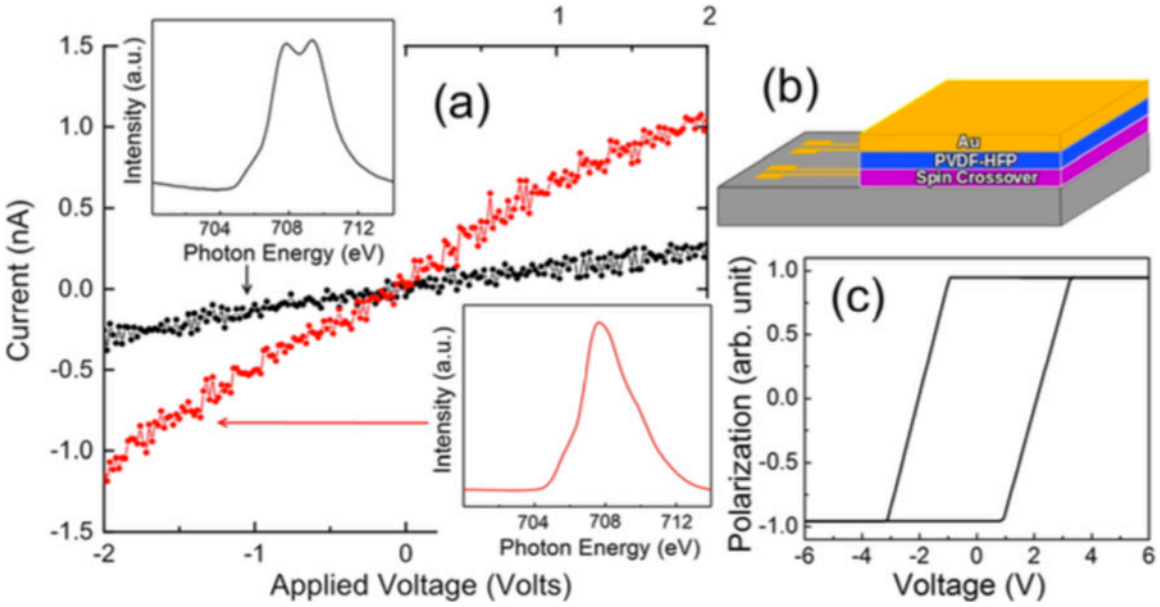

Figure 16. (a) The transport measurement and indications of conductance change associated with the spin state switching. The insets are the XAS spectra across the Fe $2p_{3/2}$ core level indicating a change from the mostly low spin state to the high spin state for the $[Fe(H_2B(pz)_2)_2bipy]$ on the organic ferroelectric polyvinylidene fluoride hexafluoropropylene (PVDF-HFP) polarized towards the $[Fe(H_2B(pz)_2)_2bipy]$ (red) or away (black). (b) The schematics of the transistor device. (c) The hysteresis loop of the ferroelectric substrate. Reprinted from [56], with the permission of AIP Publishing.

pz = tris(pyrazol-1-yl)-borohydride and bipy = 2,2′-bipyridine, on top of organic ferroelectric substrate PVDF-TrFE, the direction of the interface dipole moment will lock the spin state of $[Fe(H_2B(pz)_2)_2bipy]$ into either the high spin or low spin configuration depending on the direction of the moment, as schematically illustrated in figure 15, and more recently repeated on the molecular ferroelectric polyvinylidene fluoride hexafluoropropylene (PVDF-HFP) [56]. This result was explored further to demonstrate isothermal reversible spin state switching, at room temperature, through an applied voltage [56]. Molecular thin films of the spin crossover complex $[Fe(H_2B(pz)_2)_2bipy]$ grown adjacent to the organic ferroelectrics PVDF-HF and croconic acid, were seen to have nonvolatile locking of the spin state, but the spin state could then be manipulated by an applied electric field [56]. The spin state was directly probed by x-ray absorption spectroscopy, but the spin state switching was seen to be accompanied by a conductance change [56]. The high spin state was seen to have

higher conductance than the low spin state (figure 16). There is now at least one example of voltage controlled nonvolatile reversible spin state switching at room temperature.

7. Conclusion

Obviously, there is now considerable evidence that gated molecular spin devices, using single (or only a few) molecule magnets, can be fabricated. First, although electromigration and break-junction device techniques have been widely used for the fabrication of single molecule devices, the success rate still remains low. It appears that only a small fraction of the devices fabricated showed the desired single electron transport characteristics such as Coulomb blockade and Kondo effects [44–50]. Nor is it easy to establish beyond any shadow of doubt whether the single molecule devices are indeed restricted to a single molecule, as opposed to few-molecule device. For molecules coupled, i.e. in electrical contact, to the metal, there might be a size mismatch so fine tuning the devices source-drain gap, to fit the molecule of interest and then inserting the molecule correctly, may be regarded as impressive technical challenges. Avoiding screening, by the high electron density of the adjacent metal electrodes can be done by chemical means, as indicated above, but by no means can one completely avoid a closing of the HOMO–LUMO gap due to proximity of the adjacent metal. Using organic electrodes such as graphene or carbon nanotubes may solve this problem and broaden the choices of ligand groups, while possibly providing a route to more controlled if not more facile charge injection. Several groups have begun utilizing this idea and some progress has been made [54, 63]. Furthermore, so far there is no way to precisely control the orientation of the molecule, when embedding a local moment molecule in the region between the source/drain electrodes, and how this influences the easy axis of the molecular magnetic anisotropy still remains unclear.

Another big issue to address is that all the single molecule devices reviewed here work only at very low temperatures (far below 40 K). Electrical tuning of the molecular spin states using gate voltage is of great importance, in molecular spintronics, but to be a 'true' device applicable to memory applications, this has to work at room temperature. The grand challenge is to achieve the electric tuning of the molecular spin states in a nonvolatile and reversible way around room temperature, so that better low power consumption spintronic devices can be designed and utilized. The specific challenges include (1) the ability to make a thin film, (2) the ability to 'lock' the spin state, i.e. achieve nonvolatility, (3) the ability to isothermally 'unlock' and switch the spin state, ideally with voltage, (4) obtain a usable readout mechanism, like a conductance change with spin state, which then needs to be accompanied by (5) high on/off ratios, (6) room temperature operation, (7) reasonably fast read and write operations (ideally 1 ns or less), and (8) sufficiently robust to survive 10^{16} switches. As yet, not all these conditions have been met in a working molecular spintronics device. Yet there is, in fact, considerable progress in meeting the challenges that need to be met to build scalable molecular spintronic memory.

Acknowledgments

This research was supported by the National Science Foundation through NSF-Chem 1856614. The authors have benefitted from numerous discussions with Prof. Xiaoshan Xu.

ORCID iDs

Guanhua Hao https://orcid.org/0000-0003-3281-6816
P A Dowben https://orcid.org/0000-0002-2198-4710

References

[1] Cornia A and Seneor P 2017 The molecular way *Nat. Mater.* **16** 505–6
[2] Ludwig E, Naggert H, Kalläne M, Rohlf S, Kröger E, Bannwarth A, Quer A, Rossnagel K, Kipp L and Tuczek F 2014 Iron(II) spin-crossover complexes in ultrathin films: electronic structure and spin-state switching by visible and vacuum-UV light *Angew. Chem., Int. Ed. Engl.* **53** 3019–23
[3] Rotaru A, Dugay J, Tan R P, Guralskiy I A, Salmon L, Demont P, Carrey J, Molnár G, Respaud M and Bousseksou A 2013 Nano-electromanipulation of spin crossover nanorods: towards switchable nanoelectronic devices *Adv. Mater.* **25** 1745–9
[4] Rotaru A, Gural'skiy I A, Molnár G, Salmon L, Demont P and Bousseksou A 2012 Spin state dependence of electrical conductivity of spin crossover materials *Chem. Commun.* **48** 4163–5
[5] Ruiz E 2014 Charge transport properties of spin crossover systems *Phys. Chem. Chem. Phys.* **16** 14–22
[6] Kuch W and Bernien M 2017 Controlling the magnetism of adsorbed metal–organic molecules *J. Phys.: Condens. Matter* **29** 023001
[7] Miyamachi T *et al* 2012 Robust spin crossover and memristance across a single molecule *Nat. Commun.* **3** 938
[8] Gopakumar T G, Matino F, Naggert H, Bannwarth A, Tuczek F and Berndt R 2012 Electron-induced spin crossover of single molecules in a bilayer on gold *Angew. Chem., Int. Ed. Engl.* **51** 6262–6
[9] Zhang X *et al* 2017 Locking and unlocking the molecular spin crossover transition *Adv. Mater.* **29** 1702257
[10] Molnár G, Rat S, Salmon L, Nicolazzi W and Bousseksou A 2018 Spin crossover nanomaterials: from fundamental concepts to devices *Adv. Mater.* **30** 1703862
[11] Pronschinske A, Chen Y, Lewis G F, Shultz D A, Calzolari A, Buongiorno Nardelli M and Dougherty D B 2013 Modification of molecular spin crossover in ultrathin films *Nano Lett.* **13** 1429–34
[12] Mahfoud T, Molnár G, Bonhommeau S, Cobo S, Salmon L, Demont P, Tokoro H, Ohkoshi S, Boukheddaden K and Bousseksou A 2009 Electric-field-induced charge-transfer phase transition: a promising approach toward electrically switchable devices *J. Am. Chem. Soc.* **131** 15049–54
[13] Mahfoud T, Molnár G, Cobo S, Salmon L, Thibault C, Vieu C, Demont P and Bousseksou A 2011 Electrical properties and non-volatile memory effect of the $[Fe(HB(pz)_3)_2]$ spin crossover complex integrated in a microelectrode device *Appl. Phys. Lett.* **99** 053307

[14] Prins F, Monrabal-Capilla M, Osorio E A, Coronado E and van der Zant H S J 2011 Room-temperature electrical addressing of a bistable spin-crossover molecular system *Adv. Mater.* **23** 1545–9

[15] Lefter C, Davesne V, Salmon L, Molnár G, Demont P, Rotaru A and Bousseksou A 2016 Charge transport and electrical properties of spin crossover materials: towards nanoelectronic and spintronic devices *Magnetochemistry* **2** 18

[16] Smullen C W, Nigam A, Gurumurthi S and Stan M R 2011 The STeTSiMS STT-RAM simulation and modeling system *2011 IEEE/ACM Int. Conf. on Computer-Aided Design IEEE Explore, INSPEC Accession Number: 12437597* pp 318–25

[17] Wang R, Jiang L, Zhang Y, Wang L and Yang J 2015 Selective restore: an energy efficient read disturbance mitigation scheme for future STT-MRAM *2015 52nd ACM/EDAC/ IEEE Design Automation Conf., IEEE Xplore, INSPEC Accession Number: 15311851*

[18] Chun K C, Zhao H, Harms J D, Kim T-H, Wang J-P and Kim C H 2013 A scaling roadmap and performance evaluation ofin-plane and perpendicular MTJ based STT-MRAMs for high-density cache memory *IEEE J. Solid-State Circuits* **48** 598

[19] Jiang X *et al* 2019 Tunable spin-state bistability in a spin crossover molecular complex *J. Phys.: Condens. Matter* **31** 315401

[20] Bogani L and Wernsdorfer W 2008 Molecular spintronics using single-molecule magnets *Nat. Mater.* **7** 179–86

[21] Christou G, Gatteschi D, Hendrickson D N and Sessoli R 2000 Single-molecule magnets *MRS Bull.* **25** 66–71

[22] Lis T 1980 Preparation, structure, and magnetic properties of a dodecanuclear mixed-valence manganese carboxylate *Acta Crystallogr.* B **36** 2042–6

[23] Caneschi A, Gatteschi D, Sessoli R, Barra A L, Brunel L C and Guillot M 1991 Alternating current susceptibility, high field magnetization, and millimeter band EPR evidence for a ground $S = 10$ state in $[Mn_{12}O_{12}(CH_3COO)_{16}(H_2O)_4].2C H_3COOH.4H_2O$ *J. Am. Chem. Soc.* **113** 5873

[24] Sessoli R, Tsai H L, Schake A R, Wang S, Vincent J B, Folting K, Gatteschi D, Christou G and Hendrickson D N 1993 High-spin molecules: $[Mn_{12}O_{12}(O_2CR)_{16}(H_2O)_4]$ *J. Am. Chem. Soc.* **115** 1804–16

[25] Sessoli R, Gatteschi D, Canesch A and Novak M A 1993 Magnetic bistability in a metal-ion cluster *Nature* **365** 141–3

[26] Guo F-S, Day B M, Chen Y-C, Tong M-L, Mansikkamäki A and Layfield R A 2018 Magnetic hysteresis up to 80 kelvin in a dysprosium metallocene single-molecule magnet *Science* **362** 1400–3

[27] Perrin M L, Burzurí E and van der Zant H S J 2015 Single-molecule transistors *Chem. Soc. Rev.* **44** 902–19

[28] Zimbovskaya N A 2013 *Transport Properties of Molecular (Junctions Springer Tracts in Modern Physics)* (Berlin, Heidelberg: Springer) p 254

[29] Nolting W and Ramakanth A 2009 *Quantum Theory of Magnetism* (Berlin: Springer)

[30] Gütlich P and Goodwin H A 2004 *Spin Crossover in Transition Metal Compounds* I (Berlin: Springer)

[31] Gütlich P, Garcia Y and Goodwin H A 2000 Spin crossover phenomena in Fe(ii) complexes *Chem. Soc. Rev.* **29** 419–27

[32] Cambi L and Szegö L 1931 *Ber. Deutsch Chem. Ges.* **64** 167

[33] Cambi L and Malatesta L 1937 *Ber. Deutsch Chem. Ges.* **70** 2067

[34] Kyatskaya S, Galán Mascarós J R, Bogani L, Hennrich F, Kappes M, Wernsdorfer W and Ruben M 2009 Anchoring of rare-earth-based single-molecule magnets on single-walled carbon nanotubes *J. Am. Chem. Soc.* **131** 15143–51

[35] Friedman J R, Sarachik M P, Tejada J and Ziolo R 1996 Macroscopic measurement of resonant magnetization tunneling in high-spin molecules *Phys. Rev. Lett.* **76** 3830–3

[36] Thomas L, Lionti F, Ballou R, Gatteschi D, Sessoli R and Barbara B 1996 Macroscopic quantum tunnelling of magnetization in a single crystal of nanomagnets *Nature* **383** 145–7

[37] Park H, Lim A K L, Alivisatos A P, Park J and McEuen P L 1999 Fabrication of metallic electrodes with nanometer separation by electromigration *Appl. Phys. Lett.* **75** 301–3

[38] Bellec A, Lagoute J and Repain V 2018 Molecular electronics: scanning tunneling microscopy and single-molecule devices *C. R. Chim.* **21** 1287e1299

[39] Cui A, Dong H and Hu W 2015 Nanogap electrodes towards solid state single-molecule transistors *Small* **11** 6115–41

[40] Guo X (ed)2019 *Molecular-Scale Electronics, Topics in Current Chemistry Collections* (Berlin: Springer)

[41] Xiao J and Dowben P A 2009 Changes in the adsorbate dipole layer with changing d-filling of the metal (II) (Co, Ni, Cu) phthalocyanines on Au(1 1 1) *J. Phys.: Condens. Matter* **21** 052001

[42] Ishii H, Sugiyama K, Ito E and Seki K 1999 Energy level alignment and interfacial electronic structures at organic/metal and organic/organic interfaces *Adv. Mater.* **11** 605

[43] Gatteschi D and Sessoli R 2003 Quantum tunneling of magnetization and related phenomena in molecular materials *Angew. Chem., Int. Ed. Engl.* **42** 268–97

[44] Heersche H B, de Groot Z, Folk J A, van der Zant H S J, Romeike C, Wegewijs M R, Zobbi L, Barreca D, Tondello E and Cornia A 2006 Electron transport through single Mn_{12} molecular magnets *Phys. Rev. Lett.* **96** 206801

[45] Jo M-H, Grose J E, Baheti K, Deshmukh M M, Sokol J J, Rumberger E M, Hendrickson D N, Long J R, Park H and Ralph D C 2006 Signatures of molecular magnetism in single-molecule transport spectroscopy *Nano Lett.* **6** 2014–20

[46] Zyazin A S *et al* 2010 Electric field controlled magnetic anisotropy in a single molecule *Nano Lett.* **10** 3307–11

[47] Burzurí E, Zyazin A S, Cornia A and van der Zant H S J 2012 Direct observation of magnetic anisotropy in an individual Fe_4 single-molecule magnet *Phys. Rev. Lett.* **109** 147203

[48] Park J *et al* 2002 Coulomb blockade and the Kondo effect in single-atom transistors *Nature* **417** 722–5

[49] Liang W, Shores M P, Bockrath M, Long J R and Park H 2002 Kondo resonance in a single-molecule transistor *Nature* **417** 725–9

[50] Meded V, Bagrets A, Fink K, Chandrasekar R, Ruben M, Evers F, Bernand-Mantel A, Seldenthuis J S, Beukman A and van der Zant H S J 2011 Electrical control over the Fe(II) spin crossover in a single molecule: theory and experiment *Phys. Rev.* B **83** 245415

[51] Vincent R, Klyatskaya S, Ruben M, Wernsdorfer W and Balestro F 2012 Electronic read-out of a single nuclear spin using a molecular spin transistor *Nature* **488** 357–60

[52] Thiele S, Balestro F, Ballou R, Klyatskaya S, Ruben M and Wernsdorfer W 2014 Electrically driven nuclear spin resonance in single-molecule magnets *Science* **344** 1135–8

[53] Ganzhorn M, Klyatskaya S, Ruben M and Wernsdorfer W 2013 Strong spin–phonon coupling between a single-molecule magnet and a carbon nanotube nanoelectromechanical system *Nat. Nanotechnol.* **8** 165–9

[54] Lumetti S, Candini A, Godfrin C, Balestro F, Wernsdorfer W, Klyatskaya S, Ruben M and Affronte M 2016 Single-molecule devices with graphene electrodes *Dalton Trans.* **45** 16570–4

[55] Godfrin C, Ferhat A, Ballou R, Klyatskaya S, Ruben M, Wernsdorfer W and Balestro F 2017 Operating quantum states in single magnetic molecules: implementation of Grover's quantum algorithm *Phys. Rev. Lett.* **119** 187702

[56] Hao G *et al* 2019 Nonvolatile voltage controlled molecular spin state switching *Appl. Phys. Lett.* **114** 032901
[57] Aravena D and Ruiz E 2012 Coherent transport through spin-crossover single molecules *J. Am. Chem. Soc.* **134** 777–9
[58] Zapf V S, Sengupta P, Batista C D, Nasreen F, Wolff-Fabris F and Paduan-Filho A 2018 Magnetoelectric effects in an organometallic quantum magnet *Phys. Rev.* B **83** 140405
[59] Zapf V S, Kenzelmann M, Wolff-Fabris F, Balakirev F and Chen Y 2010 Magnetically induced electric polarization in an organometallic magnet *Phys. Rev.* B **82** 060402
[60] Chikara S, Gu J, Zhang X-G, Cheng H-P, Smythe N, Singleton J, Scott B, Krenkel E, Eckert J and Zapf V S 2019 Magnetoelectric behavior via a spin state transition *Nat. Commun.* **10** 4043
[61] Zhao W, Zou D, Sun Z, Xu Y, Ji G, Yu Y and Yang C 2019 Spin logic gates operated by protonation and magnetism in molecular combinational circuits *Adv. Theory Simul.* **2** 1900057
[62] Zhang X, Palamarciuc T, Létard J-F, Rosa P, Lozada E V, Torres F, Rosa L G, Doudin B and Dowben P A 2014 The spin state of a molecular adsorbate driven by the ferroelectric substrate polarization *Chem. Commun.* **50** 2255
[63] El Abbassi M *et al* 2019 Robust graphene-based molecular devices *Nat. Nanotechnol.* **14** 957–61